International Journal of Biological Macromolecules 322 (2025) 146679

Contents lists available at ScienceDirect

International Journal of Biological Macromolecules

journal homepage: www.elsevier.com/locate/ijbiomac

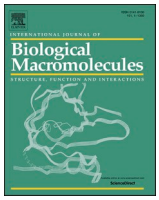

Freeze-dryable inks combining chitosan nanofibers and hyaluronic acid for extrusion bioprinting

Ryo Hirami , Shinji Sakai *

Department of Materials Engineering Science, Graduate School of Engineering Science, The University of Osaka, Toyonaka, Osaka 560-8531, Japan

ARTICLE INFO

Keywords:
Three-dimensional bioprinting
Freeze-dryable ink
Chitosan nanofibers

ABSTRACT

Freeze-dryable inks offer significant advantages for bioprinting, such as long-term biochemical and biophysical stability with minimal risks of hydrolysis, denaturation, and microbial contamination. In this study, we developed inks that can be stored in a ready-to-use, freeze-dried form by incorporating chitosan nanofibers (ChitoNFs), sodium hyaluronic acid (HA-Na), and phenolated HA (HA-Ph). HA-Na and HA-Ph effectively inhibited ChitoNF aggregation during drying. Upon rehydration, the developed inks exhibited shear-thinning behavior and underwent horseradish peroxidase-catalyzed gelation. The optimization of the ChitoNF, HA-Na, and HA-Ph concentrations enabled precise control of the viscosity, gelation time, and hydrogel stiffness after rehydration. Using 0.8 w/v% HA-Na, 0.2 w/v% HA-Ph, and 1.5 w/v% ChitoNF, we achieved high-fidelity three-dimensional printing of constructs. Furthermore, the incorporation of 0.5 w/v% phenolated gelatin supported the encapsulation of 10 T1/2 fibroblasts, resulting in more than 90 % viability and a 3.1-fold increase in mitochondrial activity over 7 d. Our findings revealed that pre-mixed, freeze-dryable ChitoNF–HA-Na/HA-Ph bioinks offer a practical and innovative solution for bioprinting. By ensuring long-term storability, quantitative retention of print fidelity and cytocompatibility after rehydration, and simplified logistics for clinical translation, they address unmet needs in current bioink technologies.

1. Introduction

Nanofibers exhibit exceptional properties, such as high strength and elasticity, and are valuable for various applications [1,2]. To maximize their advantages, their uniform dispersion in a matrix is essential [3,4]. Bioprinting is an advanced technology for fabricating cell-laden three-dimensional (3D) structures using bioinks and 3D printers. Nanofiber additives can enhance bioprintability in extrusion-based applications and reinforce the mechanical strength of bioprinted constructs, both of which are crucial for fabricating stable and functional tissue structures [5–9]. However, conventional nanofiber-containing inks encounter significant challenges, particularly aggregation during storage, which hampers redispersion and degrades printability after rehydration [10,11].

Bioinks are typically composed of biomolecules such as polysaccharides and proteins [12,13]. Preserving these components from degradation, including hydrolysis, denaturation, and bioactivity loss during storage, is vital for successful bioprinting. Among available storage methods, freeze-drying is more effective than refrigeration or freezing, because it prevents hydrolysis and maintains bioink integrity [14]. However, owing to strong intermolecular interactions such as hydrogen bonding and van der Waals forces, nanofiber-based inks tend to form irreversible aggregates during the freeze-drying process. This aggregation leads to poor redispersion, resulting in inconsistent bioink viscosity and compromised printability [15,16]. Hence, the development of ready-to-use freeze-dried inks containing nanofibers is required.

Various nanofiber materials have been incorporated into bioinks, and their value has been demonstrated based on the properties of each material [8,9,17]. Chitosan nanofibers (ChitoNFs), which are prepared by grinding chitosan powder suspended in an aqueous solution, have been proven to be effective additives for bioinks [8]. Chitosan is a polysaccharide derived from chitin, which is found in the exoskeletons of crustaceans and insects as well as in the cell walls of fungi, including mushrooms. Chitosan has been extensively investigated for its biocompatibility, biodegradability, and antimicrobial properties [18,19] in various biomedical applications, such as tissue engineering [20,21], drug delivery [22,23], and wound dressing [24,25]. Practical applications require ink storage before bioprinting; however, to the best of our

* Corresponding author.
E-mail address: sakai@cheng.es.osaka-u.ac.jp (S. Sakai).

https://doi.org/10.1016/j.ijbiomac.2025.146679
Received 1 March 2025; Received in revised form 22 July 2025; Accepted 6 August 2025
Available online 7 August 2025

knowledge, no study has systematically addressed the challenge of irreversible aggregation in nanofiber-based inks during freeze-drying. Furthermore, the combination of ChitoNFs and hyaluronic acid (HA) or its derivatives in a freeze-dryable formulation remains unexplored, despite their complementary functions: HA is a naturally occurring polysaccharide with excellent biocompatibility [26,27] and tunable rheology, while ChitoNFs offer superior mechanical reinforcement [8].

To address these challenges, we developed a novel ready-to-use freeze-dryable bioink formulation by combining ChitoNFs and HA, including its derivatives. The formulation was designed to achieve enhanced dispersion stability, tunable rheological properties, and high print fidelity after rehydration. The key innovation lies in leveraging the electrostatic interactions between the positively charged ChitoNFs and negatively charged HA, including its derivatives, to suppress irreversible aggregation of nanofibers during freeze-drying. This strategy not only preserves nanofiber dispersibility but also enhances shear-thinning behavior and structural integrity upon rehydration (Fig. 1).

The printability and cytocompatibility of the optimized formulation were evaluated and its hydrogel-forming capability was investigated via horseradish peroxidase (HRP)-mediated cross-linking of phenolated HA (HA-Ph). In the presence of hydrogen peroxide, HRP catalyzes the oxidation of the phenol (Ph) groups on the polymers, generating phenoxy radicals that form covalent cross-links, thus yielding a 3D hydrogel network. HRP-mediated hydrogelation has been successfully demonstrated for both nanofiber-containing [8,9] and nanofiber-free bioinks [28,29]. Unlike previous studies that have focused only on freshly prepared nanofiber-containing bioinks [30,31], including those gellable through HRP-mediated reactions, our study demonstrated the feasibility of freeze-dried storage while retaining key functional properties. This work represents the first systematic attempt to overcome freeze-drying-induced nanofiber aggregation by harnessing electrostatic interactions between ChitoNFs and HA, including its derivatives, resulting in a formulation with enhanced dispersion, storage stability, and printability for bioprinting applications. The insights gained in this study contribute to the development of robust, scalable bioinks for extrusion bioprinting and tissue engineering.

2. Materials and methods

2.1. Materials

ChitoNFs (diameter of 20–50 nm) prepared using a high-pressure water jet system [32] were purchased from Sugino Machine (Tokyo, Japan) (Fig. 1b). Tyramine hydrochloride and 3-(4-hydroxyphenyl) propionic acid (HPP) were obtained from Tokyo Chemical Industry Co. Ltd. (Tokyo, Japan). Ovine catalase, HRP (140 units/mg), H_2O_2 aqueous solution (30 w/w%), lactobionic acid, N-hydroxysuccinimide (NHS), hydrogen chloride (HCl) aqueous solution, and dimethylformamide (DMF) were purchased from Fujifilm Wako Pure Chemical Corp. (Osaka, Japan). 2-Morpholinoethanesulfonic acid monohydrate (MES), propidium iodide (PI), and Cell Counting Kit-8 for evaluating mitochondrial activity were purchased from Dojindo (Kumamoto, Japan). Sodium HA (HA-Na) with a molecular weight of approximately 1000 kDa was obtained from Kewpie (Tokyo, Japan). Chitosan (chitosan LL, average molecular weight of 8.3×10^4 Da, deacetylation degree 75 %) was provided by Yaizu Suisankagaku Industry (Shizuoka, Japan). Bovine skin gelatin (Gelatin Type B), *N*,*N*,*N*′,*N*′-tetramethylethylenediamine (TEMED), and poly(ethylene glycol) (PEG, MW 900 kDa) were purchased from Sigma-Aldrich (St. Louis, MO, USA). Water-soluble carbodiimide hydrochloride (WSCD·HCl) and calcein AM were obtained from the Peptide Institute (Osaka, Japan) and Nacalai Tesque Inc. (Kyoto, Japan), respectively. Mouse fibroblast cell line 10 T1/2 cells obtained from the RIKEN Cell Bank (Ibaraki, Japan) were cultured in Dulbecco's modified Eagle medium (DMEM, Nissui Pharmaceutical Co., Ltd., Tokyo, Japan) with 10 % fetal bovine serum in a humidified environment (37 °C, 5 % CO_2).

2.2. Synthesis of phenolated polymers

HA-Ph, phenolated gelatin (Gelatin-Ph), and phenolated chitosan (Chitosan-Ph) were synthesized via WSCD/NHS-mediated carbodiimide coupling reactions according to established protocols [33,34]. Briefly, HA-Ph was synthesized as follows: HA-Na was dissolved at 0.75 w/v% in a 0.1 M MES buffer solution (pH 6). WSCD·HCl, NHS, and tyramine hydrochloride were dissolved in the polymer solution at 28, 27, and 70

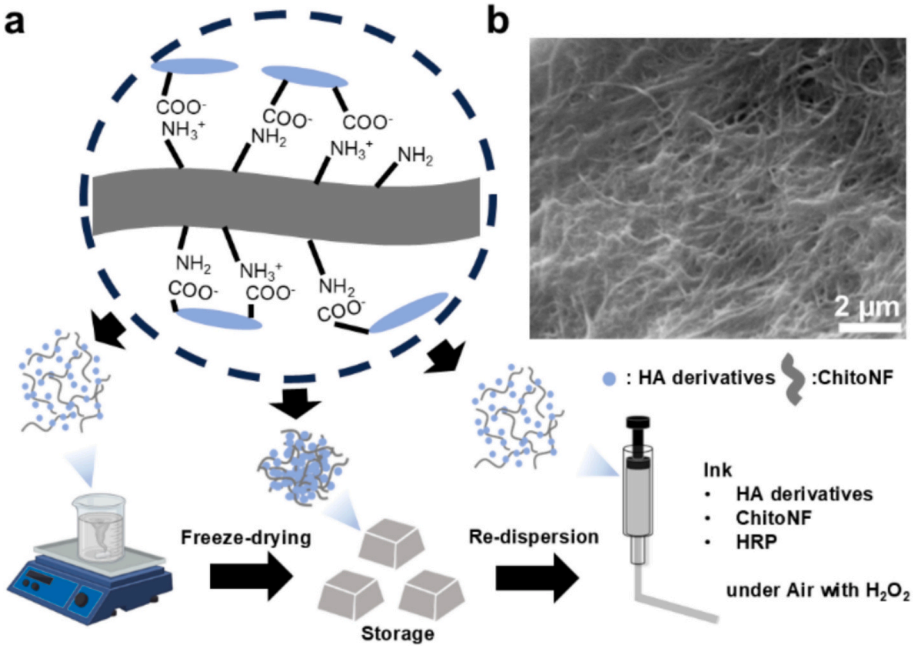

Fig. 1. a) Schematic representation of the pre-mix process to obtain inks containing ChitoNFs and HA derivatives. These inks undergo gelation via HRP-mediated cross-linking. b) Scanning electron microscope image of ChitoNF.

mM, respectively. After stirring for 20 h at room temperature, the solution was dialyzed against deionized water and freeze-dried. Gelatin-Ph was synthesized as follows: Gelatin Type B was dissolved at 4.0 w/v% in a mixture of water and DMF (v/v = 1.5, pH 4.7). WSCD·HCl, NHS, and HPP were dissolved in the polymer solution at 77, 111, and 79 mM, respectively. After stirring for 20 h at room temperature, the solution was dialyzed against deionized water and freeze-dried. For both HA-Ph and Gelatin-Ph, dialysis was considered complete when the absorbance of the dialysate at 275 nm reached a sufficiently low level in two consecutive water changes, indicating the effective removal of unreacted phenol-containing compounds. Chitosan-Ph was synthesized as follows: Chitosan was dissolved at 7.0 w/v% in a 20 mM HCl aqueous solution, followed by the addition of TEMED at 172 mM. The pH of the solution was adjusted to 4. WSCD·HCl, HPP, and lactobionic acid were dissolved in the polymer solution at 52, 90, and 1.1 mM, respectively. After stirring for 20 h at room temperature, Chitosan-Ph was precipitated with an excess amount of acetone, washed with ethanol, and vacuum dried. The introduction of Ph groups into each polymer was quantified by measuring the absorbance of a 0.1 w/w% aqueous solution at 275 nm using standards of tyramine hydrochloride and HPP [35,36].

2.3. Freeze-drying

All polymer-based samples used for subsequent ink preparation were freeze-dried using a standardized protocol. The samples were first pre-frozen at −30 °C for at least 12 h, followed by freeze-drying under a vacuum pressure of 9–12 Pa for 48 h using a freeze dryer (model FDU-1110, EYELA, Tokyo, Japan). This protocol was consistently applied throughout the study to ensure complete dehydration while preserving nanofiber dispersibility.

2.4. Viscoelastic properties

The viscosities, storage moduli (G'), and loss moduli (G'') of the solutions were measured at 37 °C using a rheometer (HAAKE MARS III, Thermo Fisher Scientific, MA) equipped with a parallel plate of a 40-mm diameter and 0.5-mm gap. Viscoelasticity measurements were conducted using 0.7 mL of phosphate-buffered saline (PBS, pH 7.4) containing various concentrations of HA-Na, HA-Ph, Gelatin-Ph, Chitosan-Ph, PEG, and ChitoNF. The solutions were prepared using two distinct methods: the pre-mix process, where each polymer and ChitoNFs were freeze-dried together before re-dispersion, and the post-mix process, where they were freeze-dried separately before re-dispersion. The viscosities, storage modulus (G'), and loss modulus (G'') of the re-dispersed solutions obtained from each process and before freeze-drying were measured to explore the effects of the pre- and post-mix processes. The viscosity was measured at a shear rate of 1–1000 s^{-1}, whereas G was measured for a strain amplitude from 0.001 to 100 % at a constant frequency of 1 Hz in the amplitude sweep test. Additionally, a frequency sweep test was conducted from 0.1 to 10 Hz at a 1 % strain.

2.5. Dispersibility of ChitoNFs

The dispersibility of ChitoNFs was evaluated based on the degree of sedimentation of the ChitoNF aggregates. The absorbance of each solution containing 0.8 w/v% HA-Na, 0.2 w/v% HA-Ph, and 1.5 w/v% ChitoNF obtained from the pre- and post-mix processes, and prior to freeze drying, was measured at 600 nm after centrifugation (1000 rpm, 30 s).

2.6. Gelation time

The gelation time of PBS containing various concentrations of 0.8 w/v% HA-Na, 0.2–1.0 w/v% HA-Ph, 2–10 units/mL HRP, 0–1.5 w/v% ChitoNF, and 0 or 0.5 w/v% Gelatin-Ph was measured using a previously reported method [37]. Each solution (100 μL) was placed into a well of a 24-well plate, stirred at room temperature using a magnetic stirrer at 130 rpm, and exposed to air containing H_2O_2 obtained by bubbling air through a 1 M H_2O_2 aqueous solution. The gelation time was identified as the point at which the generated gel adhered to the stirrer.

2.7. Three-dimensional printing

For 3D printing, an extrusion-based system was developed by modifying a commercial 3D printer (BioX, Cellink, Gothenburg, Sweden). A mixture of PBS containing 10 units/mL HRP with 0.8 w/v% HA-Na, 0.2 w/v% HA-Ph, and 0–1.5 w/v% ChitoNF was loaded into a 2.5 mL plastic syringe. The mixture was extruded from a tapered nozzle with a 27-gauge tip (inner diameter: 0.2 mm, outer diameter: 0.6 mm) onto a substrate at a speed of 21.0 mm/s under air containing H_2O_2 (obtained by bubbling air into a 1 M H_2O_2 aqueous solution) at 37 °C. The thickness per layer of the construct was set to 0.4 mm (first layer: 0.2 mm). To assess the printability of inks, the ratio (R) of the diagonal line to the vertical line in the enclosed area of each printed lattice construct was determined.

2.8. Mechanical properties

Disk-shaped hydrogels (15 mm diameter and 1 mm thickness) were printed from PBS containing 10 units/mL HRP, various concentrations of 0.8 w/v% HA-Na, 0.2–1.0 w/v% HA-Ph, 0–1.5 w/v% ChitoNF, and 0 or 0.5 w/v% Gelatin-Ph, using the aforementioned method. These hydrogels were compressed at 6 mm/min using a tabletop material tester (EZ-test, Shimadzu, Kyoto, Japan) equipped with an 8-mm diameter probe for compression testing. The Young's modulus of each hydrogel was calculated from the strain–stress curve at strains ranging from 0 to 10 %.

2.9. Cell studies

Cell-laden disk-shaped hydrogel constructs (10 mm diameter and 1 mm thickness) were printed from PBS containing 0.8 w/v% HA-Na, 0.2 w/v% HA-Ph, 10 units/mL HRP, 0 or 1.5 w/v% ChitoNF, and 0 or 0.5 w/v% Gelatin-Ph with 10 T1/2 cells at a concentration of 2.0×10^5 cells/mL, using the aforementioned method. 10 T1/2 cells, a type of mouse fibroblast, are commonly used for cytocompatibility testing. The resulting constructs were washed with PBS and culture medium and placed in a well of a 24-well plate containing 1 mL of culture medium with 1 mg/mL catalase to degrade the remaining H_2O_2 overnight. The construct-embedded cells were then incubated in the culture medium within a humidified incubator (37 °C, 5 % CO_2) for 1, 4, and 7 d. Cell viability was evaluated via fluorescence microscopy (BZ-9000, Keyence, Osaka, Japan) after live and dead cells were stained with calcein AM and PI, respectively. The growth of the cells within the constructs was estimated by measuring the cellular mitochondrial activity per construct using Cell Counting Kit-8. The construct-embedded cells were immersed in a medium containing 1/20 (v/v) of the reagent from the assay kit. After 3 h of incubation at 37 °C, the solution was collected, and the absorbance was measured at 450 nm using a microplate reader (SpectraMax iD3, Molecular Devices, San Jose, CA, USA).

2.10. Scanning electron microscopy

Disk-shaped hydrogels (10 mm diameter and 1 mm thickness) were printed from PBS containing 0.8 w/v% HA-Na, 0.2 w/v% HA-Ph, 10 units/mL HRP, and 0 or 1.5 w/v% ChitoNF using the aforementioned method. The obtained hydrogels were rapidly frozen using liquid nitrogen and then freeze-dried. The cross sections of the dried products were sputter coated with a thin layer of gold and observed using a scanning electron microscope (SEM, JCM-6000 plus, JEOL, Tokyo, Japan).

2.11. Statistical analysis

All the experiments were performed in triplicate unless otherwise noted. The data are presented as means ± standard deviations. Statistical analysis was performed using OriginPro 2023b (OriginLab Corporation, Northampton, MA, USA). One-way ANOVA followed by Tukey's HSD test was used to assess differences among multiple groups. A p-value of less than 0.05 was considered statistically significant.

3. Results and discussion

3.1. Polymer-Ph synthesis

The introduction of Ph groups into each polymer was confirmed via ^{1}H NMR spectroscopy. Characteristic signals corresponding to the aromatic protons of the Ph groups were observed at ~7 ppm, indicating successful polymer-Ph synthesis (Fig. 2). The Ph group content was determined from the UV–vis spectra and the characteristic absorption peak at 275 nm, which corresponds to the Ph group. HA-Ph, Gelatin-Ph, and Chitosan-Ph solutions (0.1 w/v% for HA-Ph and Gelatin-Ph and 0.3 w/v% for Chitosan-Ph, Fig. S1) exhibited Ph contents of 2.8×10^{-4}, 9.8×10^{-5}, and 4.5×10^{-5} mol-Ph/g, respectively.

The Ph group content plays a critical role in controlling the crosslinking density of the bioink [38]. In HA-Ph, a higher Ph content is expected to enhance gelation efficiency, while in Chitosan-Ph, it may influence the viscoelastic properties of the resulting bioink.

3.2. Viscoelastic properties of the solutions

The viscoelastic properties of inks are crucial for their accurate deposition and printability in extrusion-based bioprinting [39]. Shear-thinning behavior, where viscosity decreases under shear stress, is particularly desirable in inks for extrusion-based bioprinting, because it facilitates smooth ink flow through the nozzle and ensures accurate and controlled deposition. Moreover, shear-thinning inks minimize the mechanical stress on cells during printing, thereby preserving high cell viability and functionality [40,41].

First, we investigated the impact of ChitoNF addition on the viscoelastic properties of solutions without freeze-drying. As shown in Fig. 3a, the viscosity of a mixture of 0.8 w/v% HA-Na and 0.2 w/v% HA-Ph increased with increasing ChitoNF content. At a shear rate of 1 s^{-1}, the viscosities of the solutions containing 1.0 and 1.5 w/v% ChitoNF were three- and six-times higher than those of the solutions without ChitoNFs, respectively. The increased viscosity at lower shear rates indicates that ChitoNFs enhanced the shear-thinning behavior of the HA-based solution. Additionally, in the 0.1–10 Hz frequency sweep test of the solution containing 0.8 w/v% HA-Na and 0.2 w/v% HA-Ph, G' increased with increasing ChitoNF content (Fig. 3b). Conversely, the addition of 0.5 w/v% Gelatin-Ph did not significantly alter the viscosity. The viscosity of the solution slightly increased with increasing HA-Na content from 0.2 to 0.8 w/v% at HA-Na + HA-Ph = 1.0 w/v% (Fig. 3c).

These findings support the effectiveness of ChitoNF addition in enhancing the shear-thinning properties of polymer solutions, which is consistent with previous studies on the addition of ChitoNFs to chitosan solutions [8]. The underlying mechanism is attributed to the shear-induced alignment of the nanofibers. Under low shear conditions, the entanglement of ChitoNFs restricts the fluidity of the solution, whereas under high shear, the nanofibers become disentangled and align along the flow direction [8]. Moreover, this effect is observed in both anionic and cationic polymers. The insignificant effect of Gelatin-Ph on the viscoelastic properties can be attributed to the low viscosity of the 0.5 w/v% Gelatin-Ph solution (Fig. 3d). Regarding the impact of the HA-Na content, increasing the HA-Ph content reduces the hydrogen bonding between the polymers due to the introduction of phenolic groups, resulting in a reduced viscosity. A similar phenomenon was reported for methacrylated HA [42].

3.3. Effect of the pre-mix process on the dispersibility of ChitoNFs

The surface condition of nanofibers during freeze-drying is crucial for their proper re-dispersion. Missoum et al. [43] demonstrated that the addition of sodium chloride to a cellulose nanofiber solution enhanced the water re-dispersion of freeze-dried cellulose nanofibers. As shown in Fig. 4a, clear aggregation of ChitoNFs was observed in the solution prepared through the post-mix process, whereas no aggregation was observed in the solution prepared through the pre-mix process, similar to the solution prior to freeze-drying (Fig. 4a). The absorbance measurements at 600 nm further supported these observations, indicating ChitoNF aggregation in the solution prepared using the post-mix process (Fig. 4b). The absorbance of the solution obtained via the pre-mix process remained stable at 3.2 after six centrifugation cycles, similar to the solution prior to freeze-drying. Conversely, the absorbance of the solution obtained via the post-mix process decreased from 2.2 to 1.9 as the number of centrifugation cycles increased, indicating sedimentation of the ChitoNF aggregates in the solution (Fig. 4b). This significant difference can be attributed to the electrostatic interactions between ChitoNFs, HA-Na, and HA-Ph during freeze-drying, which likely prevented strong intermolecular interactions such as hydrogen bonding and van der Waals forces between ChitoNFs. The uneven dispersion of nanofibers after rehydration can lead to viscosity reduction and nozzle clogging;

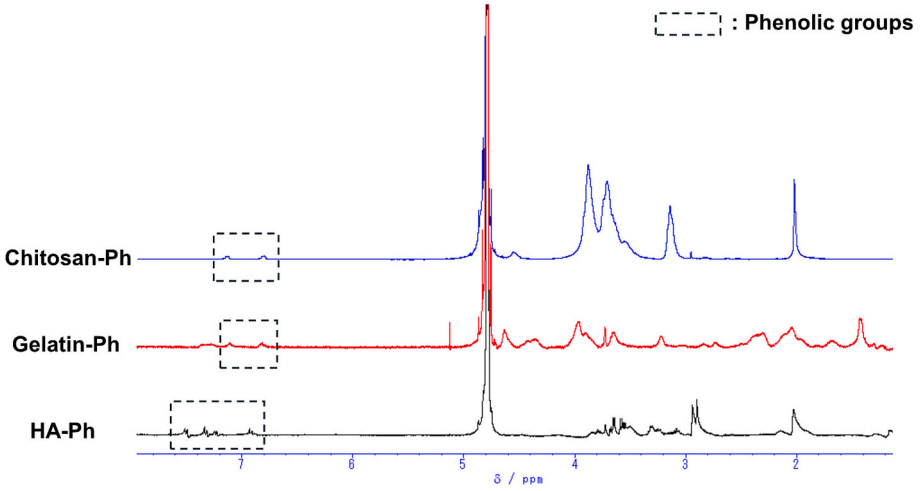

Fig. 2. ^{1}H NMR spectra of HA-Ph, Gelatin-Ph, and Chitosan-Ph in DMSO-d_6.

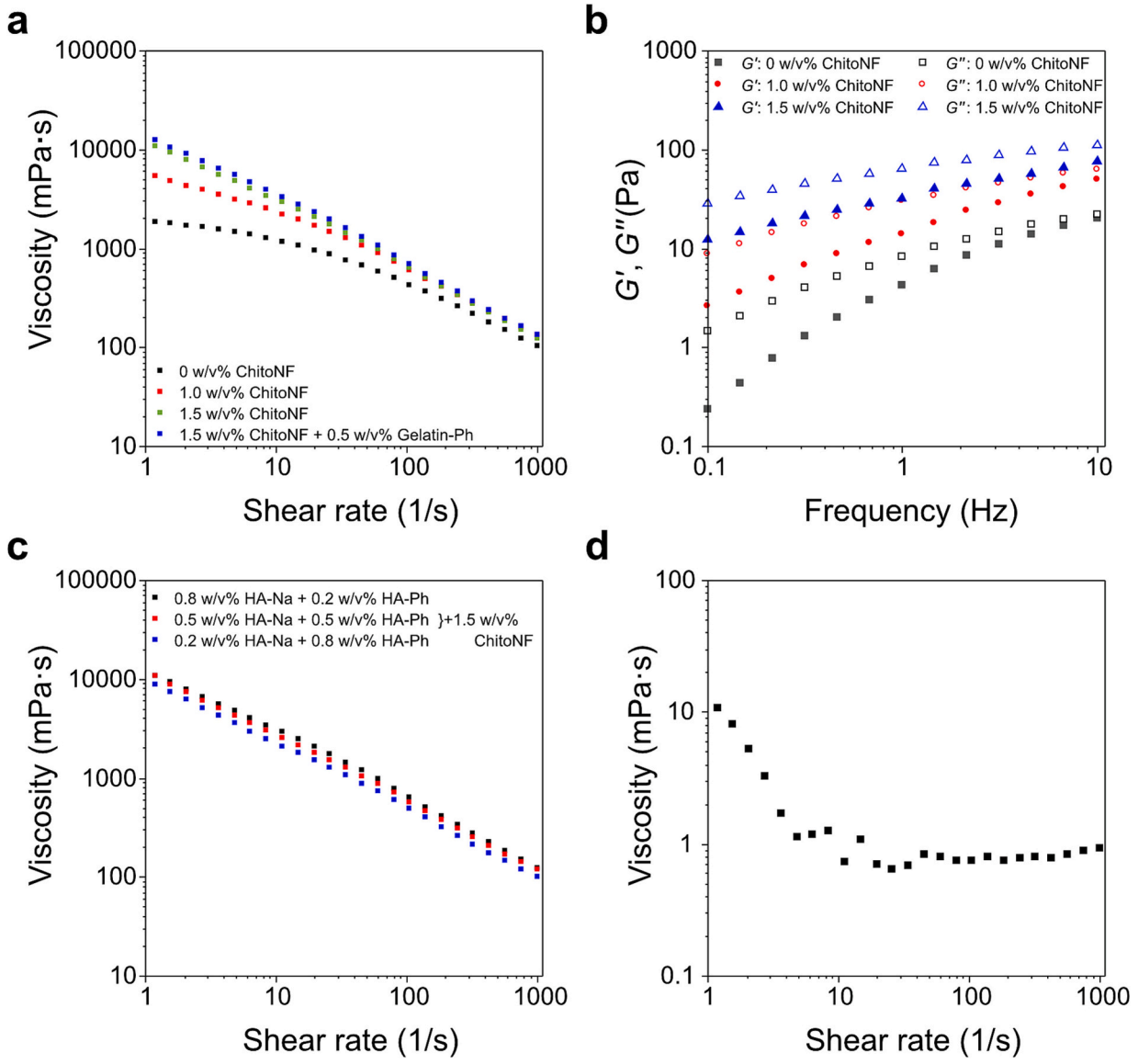

Fig. 3. Shear rate-viscosity, frequency-*G′* and *G″* profiles of solutions at 37 °C. Effects of the a), b) ChitoNF content in the solution containing 0.8 w/v% HA-Na and 0.2 w/v% HA-Ph, and c) ratio of HA-Na and HA-Ph in the solution containing 1.5 w/v% ChitoNF. d) Shear rate-viscosity profile of the solution consisting of 0.5 w/v% Gelatin-Ph.

therefore, the pre-mix process, which suppresses ChitoNF aggregation more effectively than the post-mix process, represents a promising approach for improving drying efficiency.

3.4. *Effect of the pre-mix process on the viscoelastic properties*

The effects of the ink preparation processes on the viscoelastic properties of the inks were investigated using either the pre- or post-mix process. A solution containing 0.8 w/v% HA-Na, 0.2 w/v% HA-Ph, and 1.5 w/v% ChitoNF prepared by the pre-mix process exhibited a viscosity of 5.6×10^3 mPa·s, which was approximately half of its pre-freeze-drying value, yet three times higher than that of the post-mix sample (1.9×10^3 mPa·s) at a shear rate of 1 s^{-1} (Fig. 5a).

This result indicates that the pre-mix process effectively suppressed aggregation, likely owing to the electrostatic interactions between the positively charged ChitoNFs and negatively charged HA-Na and HA-Ph. These interactions are thought to prevent strong hydrogen bonds and van der Waals forces between ChitoNFs during freeze-drying. This mechanism is consistent with previous findings on cellulose nanofibers, in which ionic interactions contributed to dispersion stability. Although the pre-mix method successfully mitigated aggregation, a significant decrease in viscosity was still be observed after freeze-drying compared with the pre-freeze-dried state. This reduction is presumably attributable to partial nanofiber bundling or disruption of the entangled network structure during the drying and rehydration process, which could not be completely prevented by electrostatic stabilization alone. Freeze-drying parameters, such as the pre-freezing temperature, freezing rate, and vacuum pressure can significantly impact the size and shape of ice crystals, as well as the kinetics of sublimation. These conditions are presumed to have induced partial structural changes in both the nanofiber network and the polymer matrix, potentially leading to the observed viscosity loss. Therefore, further optimization of these parameters may improve viscosity retention and nanofiber dispersibility after rehydration. Future work should specifically investigate whether lower freezing temperatures and controlled sublimation rates can enhance the preservation of viscosity and nanofiber dispersion. Notably, viscosity measurements revealed that the pre-mix process preserved the shear-thinning properties of the inks after freeze-drying, which supports

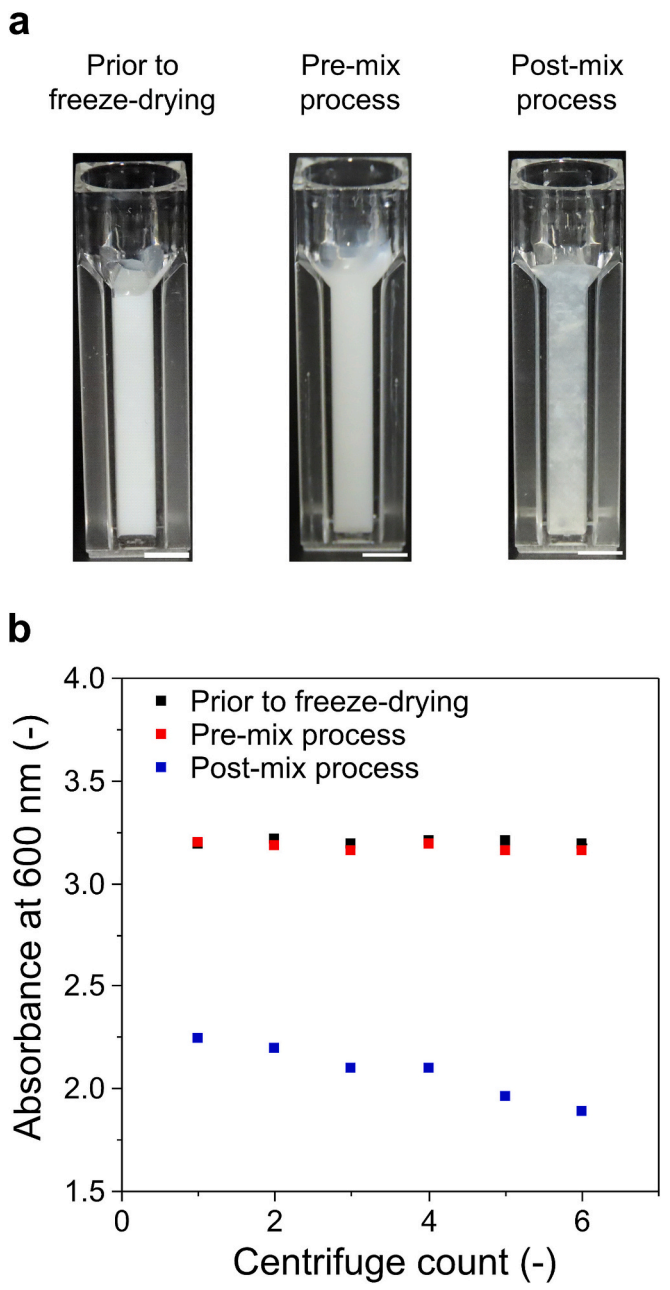

Fig. 4. a) Images and b) absorbances at 600 nm after each centrifugation of solutions containing 0.2 w/v% HA-Ph, 0.8 w/v% HA-Na, and 1.5 w/v% ChitoNF. Effect of the preparation processes. The scale bars in panel **a** are 5 mm.

the role of the charge balance in maintaining stable ink performance. However, the presence of residual aggregation suggests that further optimization of the concentrations of HA-Na and HA-Ph may be necessary to further enhance the dispersion stability. Importantly, the viscosity of the pre-mixed ink remained unchanged after three months of storage, as shown in Fig. S2, indicating excellent long-term dispersion stability. This result suggests that the electrostatic interactions formed during the pre-mix process not only prevent aggregation during freeze drying and rehydration but also contribute to sustained colloidal stability over extended storage. Such long-term viscosity retention is highly beneficial for the practical application of freeze-dried bioinks, where consistent rheological performance after rehydration is essential for reliable extrusion and printability.

To elucidate the impact of electrostatic interactions on freeze-drying, a solution containing 0.5 w/v% Chitosan-Ph as a cationic polymer, 2.0 w/v% PEG as a thickener, and 1.5 w/v% ChitoNF was prepared through a pre-mix process. Viscosity measurements before and after freeze-drying (Fig. 5b) revealed a significant decrease in viscosity after freeze-drying, compared with that of the solution containing HA-Na and HA-Ph. This suggests that the electrostatic interactions between the polymers and ChitoNFs are crucial for the proper dispersion of ChitoNFs after freeze-drying, whereas the anionic HA-Na and HA-Ph prevent intermolecular interactions between ChitoNFs, thereby suppressing their aggregation. Amplitude sweep tests were conducted on solutions containing 0.8 w/v% HA-Na, 0.2 w/v% HA-Ph, and 1.5 w/v% ChitoNF obtained from the pre-and post-mix processes and prior to freeze-drying, affording G' values that are presented in Fig. 5c. The G' value of the solution prepared via the pre-mix process exhibited a linear region with higher values than those of the post-mix sample within a strain amplitude range of 10^{-3}–10^{-1} %. This finding indicates greater structural strength and entanglement between ChitoNFs, owing to the effective dispersion of the nanofibers in the solution prepared via the pre-mix process. A similar tendency was observed in the frequency sweep test results (Fig. 5d). Although both processes resulted in a decrease in G' after freeze-drying, the decrease was less pronounced in the pre-mix sample under both amplitude and frequency sweeps. These findings highlight the superiority of the pre-mix process over the post-mix process in suppressing ChitoNF aggregation, rendering the pre-mix process a viable method for preparing freeze-dried inks. However, the pre-mix process could not completely disperse ChitoNFs to the same degree as before freeze-drying.

3.5. Gelation time

In bioprinting, the gelation time of bioinks plays a crucial role in determining the stability and accuracy of the printed structures [38,44]. Therefore, we investigated the effects of the concentration of each component (ChitoNF, HA-Ph, HRP, and Gelatin-Ph) on the gelation time.

As shown in Fig. 6, increasing the ChitoNF concentration from 0 to 1.0 w/v% did not significantly affect the gelation time, suggesting that ChitoNFs have minimal influence on the enzymatic cross-linking reaction rate at low concentrations. However, further increasing the ChitoNF content to 1.5 w/v% significantly reduced the gelation time. This phenomenon can be explained by the rheological behavior shown in Fig. 3. At 1.5 w/v% ChitoNF, the viscosity at low shear rates increased markedly (Fig. 3a), indicating the formation of a dense and entangled nanofiber network. This environment likely promotes closer proximity of phenolic moieties, thereby accelerating HRP-mediated cross-linking. Additionally, frequency sweep tests revealed a significant increase in the G' value at 1.5 w/v% ChitoNF, exceeding the G'' value across all frequencies (Fig. 3b), indicating the presence of a pre-existing elastic network structure. These physical features appear to enhance gel network formation upon enzymatic initiation, resulting in a shorter gelation time. Sakai et al. [8] reported similar effects for the gelation time of a solution containing Chitosan-Ph and ChitoNFs, attributed to HRP-mediated enzymatic cross-linking. Therefore, it is reasonable to conclude that the acceleration of gelation at high ChitoNF levels is not due to chemical reactivity changes but rather to enhanced physical proximity and nanofiber crowding effects. The gelation time of the solution without Gelatin-Ph was 5.8 ± 0.2 s, which was almost the same as that of the solution containing 0.5 w/v% Gelatin-Ph (5.6 ± 0.5 s, Fig. 6). Therefore, low concentrations of Gelatin-Ph had a minimal impact on the gelation time, similar to the viscosity.

3.6. Printability of inks

The printability of the developed inks was evaluated by printing lattice constructs (19 mm per side with a line width of 1 mm and 3 layer counts) using inks containing 0.8 w/v% HA-Na, 0.2 w/v% HA-Ph, 10 units/mL HRP, and 0–1.5 w/v% ChitoNF (Fig. 7a). Upon increasing the ChitoNF concentration, the shape of the printed area transitioned from

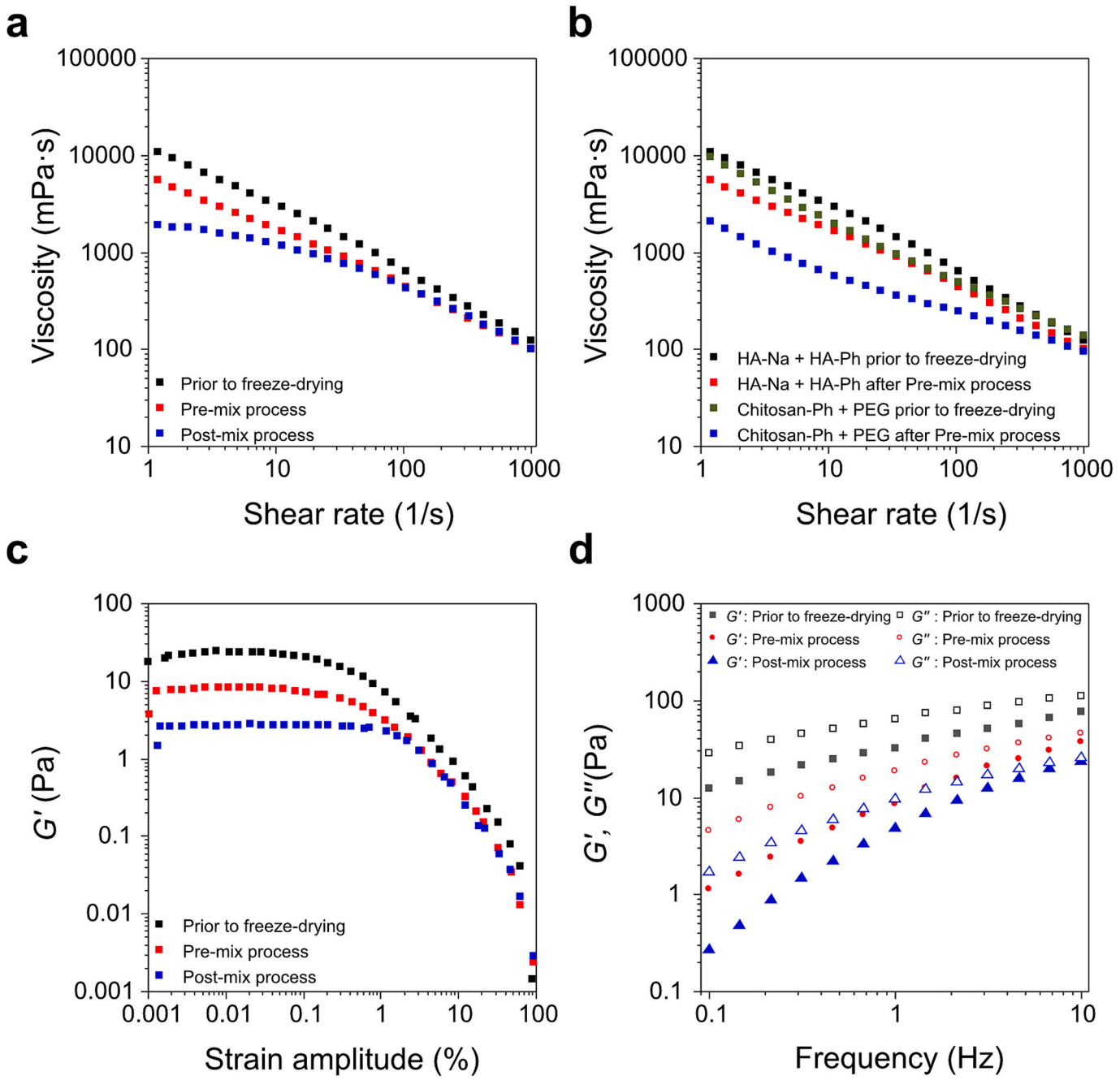

Fig. 5. Shear rate-viscosity, strain amplitude-G', and frequency-G' and G'' profiles of solutions at 37 °C. Effects of the a), c), and d) preparation processes of the solution containing 0.8 w/v% HA-Na, 0.2 w/v% HA-Ph, and 1.5 w/v% ChitoNF, and b) polymer components (0.8 w/v% HA-Na, 0.2 w/v% HA-Ph, 0.5 w/v% Chitosan-Ph, and 2.0 w/v% PEG) of the solutions containing 1.5 w/v% ChitoNF.

circular to square, with the R value approaching $\sqrt{2}$ (Fig. S3). This suggests that the ChitoNFs effectively inhibited ink spreading until gelation, resulting in excellent printability. Compared with previously reported enzymatically cross-linkable bioinks, our formulation exhibited superior printability and long-term storage capability. While Sakai et al. [8] developed chitosan-based bioinks with enhanced shear-thinning properties, they did not address long-term storage issues. Our study successfully integrated freeze-dryability without compromising ink performance. Additionally, Shin et al. [17] demonstrated the efficiency of cellulose nanofibers in improving hydrogel printability; however, their system required immediate use after preparation, whereas our bioink offers an extended shelf-life. These comparisons highlight the advantages of our freeze-dryable ChitoNF–HA bioink in ensuring both printability and storage stability.

Hollow quadrangular prism-shaped (10 × 10 mm^2, 25 layer counts) and human nose-shaped (25 × 19 mm^2, 56 layer counts) constructs were printed using various inks (Figs. S4 and 7b). A hollow quadrangular prism-shaped construct was obtained without ChitoNFs, however, it could not maintain its shape and showed poor printability owing to the spread of ink before gelation during printing. Increasing the concentration of ChitoNFs increased the ink viscosity at a low shear rate, which reduced spreading and resulted in better fidelity to the blueprint. The highest fidelity was achieved with the human nose-shaped construct containing 1.5 w/v% ChitoNF. Therefore, the addition of ChitoNFs enhanced printability, which is consistent with previous findings [8,9,17].

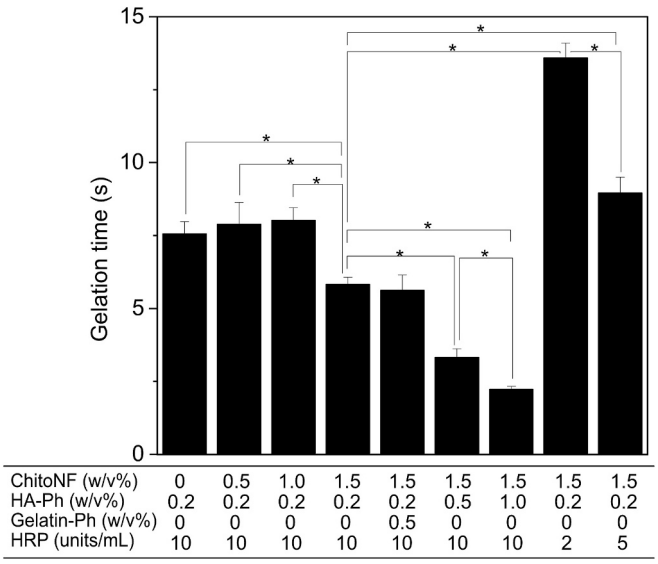

Fig. 6. Gelation time of the solutions containing 0.8 w/v% HA-Na. Effects of ChitoNF, Gelatin-Ph, HA-Ph, and HRP concentrations. The error bars represent the standard deviation ($n = 3$). *$p < 0.05$, Tukey HSD.

3.7. Mechanical properties of the hydrogels

The mechanical properties of hydrogels are crucial for 3D bioprinting because they significantly influence the cells within the printed construct [45,46]. The Young's moduli of the hydrogels increased with increasing concentrations of ChitoNFs, HA-Ph, and Gelatin-Ph, as shown in Fig. 8. The Young's modulus of the hydrogel containing 1.5 w/v% ChitoNF was 2.1 kPa, which was four times that of the ChitoNF-free hydrogel (Fig. 8). This suggests that ChitoNFs formed entanglements within the hydrogels and reinforced the hydrogel matrix. A similar trend has been reported for hydrogels containing ChitoNFs and Chitosan-Ph [8]. This increase can be attributed to the load transfer from HA-Na and HA-Ph to ChitoNFs, along with hydrogen bonding between HA and ChitoNFs. However, SEM images did not reveal any significant difference in pore size with the addition of 1.5 w/v% ChitoNF (Fig. S5). Furthermore, increasing the HA-Ph content from 0.2 to 1.0 w/v% raised the Young's modulus of hydrogels from 2.1 to 10 kPa, while the addition of 0.5 w/v% Gelatin-Ph increased it from 2.1 to 3.9 kPa (Fig. 8). An increase in the concentration of phenolated polymers facilitated strong bonding between the polymers, which aligns with previous reports [8,47]. These findings highlight the facile tunability of the stiffness of the hydrogel to the desired value, considering the cellular behavior and mechanical stability. Furthermore, this adjustable stiffness is advantageous for various tissue engineering applications.

3.8. Cytocompatibility of ChitoNFs

To investigate the cytocompatibility of the developed bioinks, we printed cell-laden constructs using three types of bioinks containing 0.8 w/v% HA-Na, 0.2 w/v% HA-Ph, and 2.0×10^5 cells/mL 10 T1/2 cells with or without 1.5 w/v% ChitoNF and 0.5 w/v% Gelatin-Ph. The construct-embedded cells were then incubated in the culture medium for 7 d. As shown in Fig. 9a, cell viability remaining above 90 % across all samples throughout the culture period, confirming the cytocompatibility of both the ink materials and the printing process. The 10 T1/2 cells enclosed in the Gelatin-Ph-free constructs were spherical and did not elongate, indicating the poor adhesive properties of the cells (Fig. 9a). Conversely, in the constructs containing Gelatin-Ph, almost all

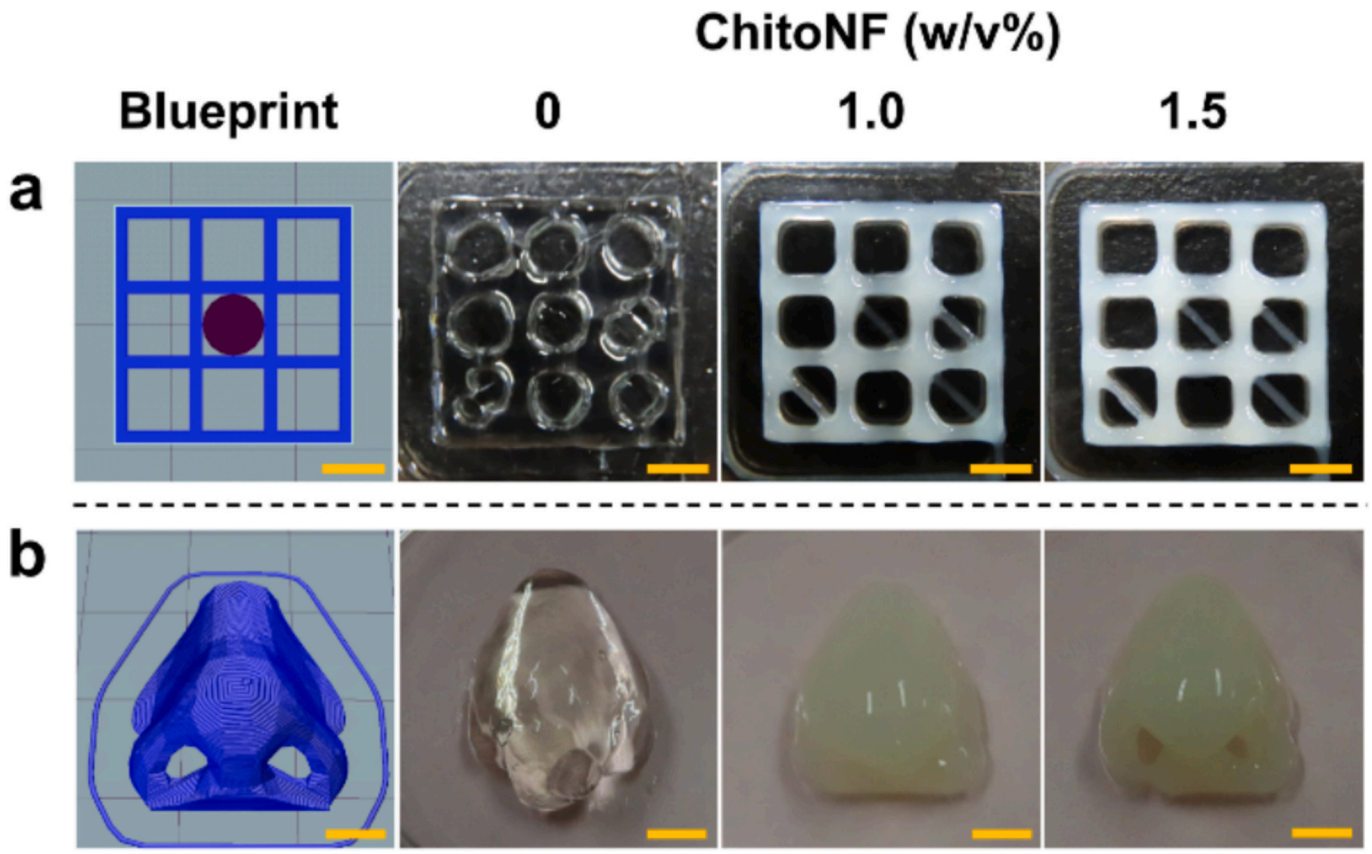

Fig. 7. Blueprints and images of the printed constructs obtained from inks containing 0.8 w/v% HA-Na, 0.2 w/v% HA-Ph, and 0–1.5 w/v% ChitoNF: a) lattice structure and b) human nose model. The scale bars are 5 mm.

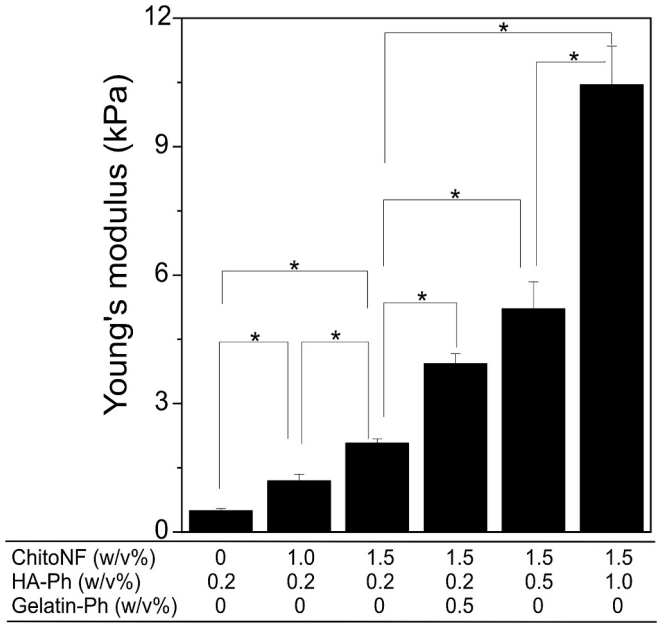

Fig. 8. Young's moduli of the hydrogels obtained from inks containing 0.8 w/v % HA-Na and 10 units/mL HRP. Effects of ChitoNF, Gelatin-Ph, and HA-Ph concentrations. The error bars represent the standard deviation ($n = 3$). *$p < 0.05$, Tukey HSD.

cells had elongated by 4 d, regardless of ChitoNFs presence (Fig. 9a). Gelatin and its derivatives are known to promote cell elongation owing to the presence of RGD sequences, which are cell adhesion sequences [35]. The addition of ChitoNFs to the construct containing HA-Na and HA-Ph and Gelatin-Ph led to slight changes in cell morphology, possibly due to the increased hydrogel stiffness, which could restrict cell spreading, as well as to the ion interactions between ChitoNFs and cell membranes.

The absence of negative effects of ChitoNFs aligns with a previous report on the cytocompatibility of ChitoNFs with Chitosan-Ph hydrogels [8]. To evaluate cell growth, mitochondrial activity assays were performed on each construct. As shown in Fig. 9b, in the absence of Gelatin-Ph (1.5 w/v% ChitoNF alone), mitochondrial activity plateaued after 4 d, indicating limited cell proliferation. In contrast, the addition of 0.5 w/v% Gelatin-Ph to hydrogels containing HA-Na and HA-Ph increased the mitochondrial activity throughout the culture period, suggesting that Gelatin-Ph significantly contributed to the promotion of cell elongation and proliferation. Furthermore, the combination of ChitoNFs and Gelatin-Ph resulted in a 3.1-fold increase in mitochondrial activity over 7 days, demonstrating a synergistic effect on enhancing cell growth. This outcome indicates that the surface charge and fiber structure of ChitoNFs, which mimic the extracellular matrix, positively influence cell behavior, ultimately increasing the mitochondrial activity per construct. Shin et al. [17] reported that the addition of cellulose nanofibers to gelatin-based hydrogels enhanced the metabolic activity of cells within the hydrogels, owing to the fibrous and porous surface of the nanofibers. Overall, the developed inks are cytocompatible and hold promise for applications in tissue engineering and regenerative medicine. To further validate the applicability of the developed freeze-dried bioink in physiologically relevant contexts, future studies should involve stem cells with differentiation potential and other primary cell types.

3.9. Limitations and perspective

This study demonstrated the feasibility of developing freeze-dryable bioinks incorporating ChitoNFs, HA-Na, and HA-Ph. Although the results are promising, several limitations must be addressed to fully validate the practical utility of the proposed ink system.

First, long-term storage stability under various environmental conditions remains untested. Although freeze-drying enhances bioink preservation, systematic evaluation of shelf-life and the retention of functional properties over time is essential for future clinical and commercial translation. Second, the role of ChitoNF morphology—particularly the aspect ratio—remains to be explored. Nanofiber length and diameter can significantly influence entanglement, dispersion, and rheological behavior; therefore, elucidating these effects could enable

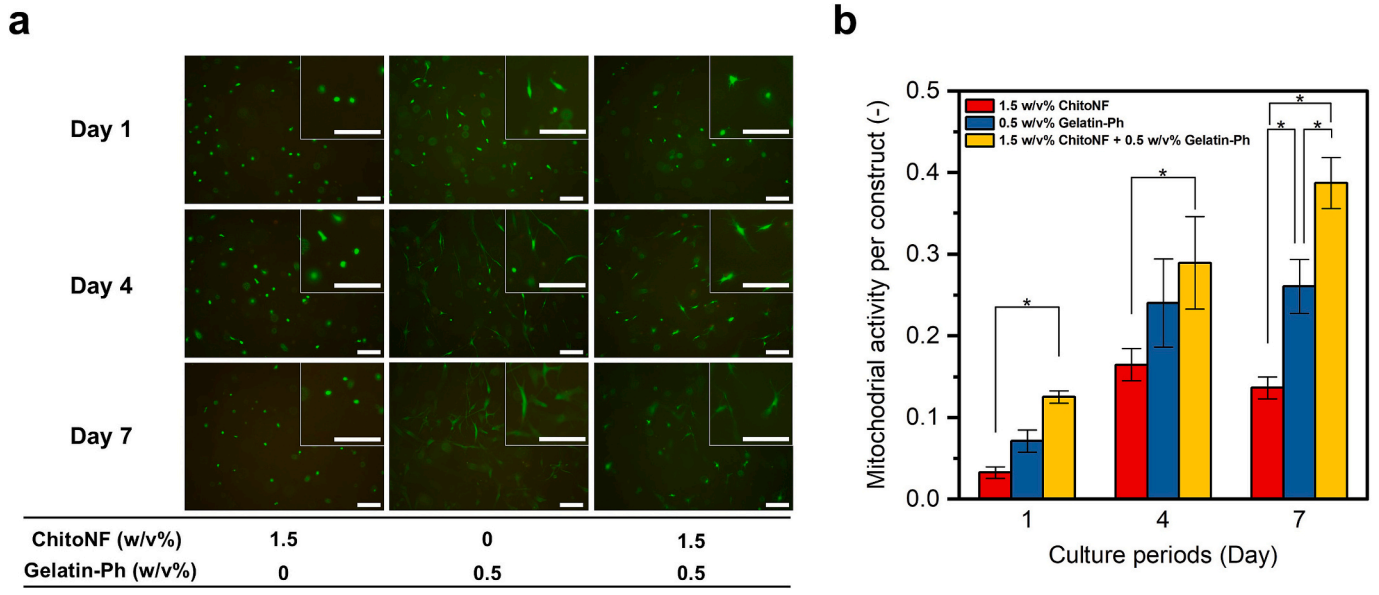

Fig. 9. Effects of ChitoNFs and Gelatin-Ph on a) the live and dead staining and morphology of enclosed cells, and b) the mitochondrial activity of cells per construct after 1–7 d of encapsulation. In (a), the cells were stained with calcein-AM (live cells, green) and propidium iodide (dead cells, red). Representative cells are shown as magnified insets in each image. In (b), mitochondrial activity was assessed using a Cell Counting Kit-8 and the absorbance was measured at 450 nm. Disk-shaped cell-laden constructs (10 mm diameter, 1 mm thickness) were prepared from inks containing 0.8 w/v% HA-Na and 0.2 w/v% HA-Ph with and without ChitoNFs and Gelatin-Ph. The scale bars are 200 μm. The error bars represent the standard deviation ($n = 3$). *$p < 0.05$, Tukey HSD. (For interpretation of the references to colour in this figure legend, the reader is referred to the web version of this article.)

further performance optimization [48,49]. Additionally, future efforts should aim to broaden the range of mechanical properties by tuning the ChitoNF concentration and cross-linking conditions to suit different tissue types. Third, the biological evaluation conducted in this study was limited to in vitro culture of fibroblasts within simple printed constructs. To better reflect physiological complexity, future investigations should include in vivo assessments of biocompatibility, degradation, and tissue remodeling in relevant models. Such studies would provide critical data for translational development.

In particular, although the freeze-dried inks retained their functional properties for at least three months, the potential impact of freeze-drying on sensitive components—such as enzyme activity and the structural integrity of biopolymers—has not been fully investigated. Future work should systematically assess the effect of the freeze-drying and rehydration processes on these components at the molecular level, to ensure consistent performance and safety in clinical applications. This will be particularly important when incorporating bioactive components in future studies.

Building on this, integrating bioactive components such as growth factors, cytokines, or extracellular matrix-derived peptides into freeze-dried bioinks may enhance their therapeutic potential by promoting cell signaling and tissue regeneration. In parallel, emerging technologies such as machine learning could facilitate the rational design of bioink formulations by predicting performance metrics based on compositional variables and printing conditions.

Notably, unlike previous studies that focused solely on freshly prepared nanofiber-based inks, our work uniquely demonstrates a freeze-dryable formulation that retains structural integrity even after storage for up to three months, highlighting its potential for real-world clinical and industrial applications. This advancement addresses a critical bottleneck for the practical implementation of nanofiber-based bioinks. Moving toward regulatory approval and clinical implementation, ensuring sterilization compatibility through the use of clinically approved materials and verifying printability with commercially available extrusion systems will be essential steps.

Overall, this study establishes a strong foundation for the development of freeze-dryable nanofiber-based bioinks. Our results demonstrate promise for enhancing extrusion bioprinting; however, some limitations require targeted research to significantly broaden their applications in tissue engineering and regenerative medicine. We anticipate that continued innovation and interdisciplinary collaboration will propel this field toward the development of more complex and functional tissue constructs suitable for clinical use.

4. Conclusion

In this study, we successfully developed a freeze-dryable bioink by pre-mixing ChitoNFs with HA-Na and HA-Ph. Pre-mixing effectively suppressed irreversible nanofiber aggregation during freeze-drying, thereby enabling homogeneous re-dispersion and ensuring consistent rheological behavior after rehydration. The optimized formulation (0.8 w/v% HA-Na, 0.2 w/v% HA-Ph, and 1.5 w/v% ChitoNF) exhibited improved shear-thinning properties and enhanced print fidelity, as demonstrated by quantitative assessments of the line width and filament collapse tests. Furthermore, the formulation retained its HRP-mediated gelation capability after freeze-drying, forming stable hydrogels under physiological conditions. The inclusion of gelatin-Ph supported cell viability and promoted the mitochondrial activity of embedded 10 T1/2 fibroblasts over a 7-d culture, confirming the cytocompatibility of the system. Importantly, rheological measurements confirmed that the viscosity properties of the freeze-dried bioink remained unchanged for at least three months of storage, underscoring its stability and potential for long-term stockpiling and distribution. These findings collectively establish that pre-mixed, freeze-dryable bioinks incorporating ChitoNFs, HA-Na, and HA-Ph provide a robust, ready-to-use platform for extrusion bioprinting.

The proposed strategy addresses key limitations of nanofiber-based bioinks, particularly with respect to storage stability and printability consistency, offering significant potential for applications in tissue engineering and regenerative medicine. Moreover, by enabling long-term preservation without compromising functionality, this approach facilitates more flexible storage and supply chain workflows. Future studies will explore broader cellular applications, extended biological evaluation periods, and compatibility with clinically approved printing systems, thereby supporting the practical deployment of freeze-dryable nanofiber bioinks in translational bioprinting.

CRediT authorship contribution statement

Ryo Hirami: Writing – original draft, Visualization, Validation, Methodology, Investigation, Formal analysis. **Shinji Sakai:** Writing – review & editing, Supervision, Resources, Project administration, Methodology, Funding acquisition, Conceptualization.

Ethical approval

This study does not include any studies with human or animal subjects performed by any of the authors.

Declaration of competing interest

The authors declare that there is no conflict of interest.

Acknowledgment

This work was supported by the Adaptable and Seamless Technology Transfer Program through Target-driven R&D (A-STEP) from the Japan Science and Technology Agency (JST), Japan Grant Number JPMJTR234C.

Appendix A. Supplementary data

Supplementary data to this article can be found online at https://doi.org/10.1016/j.ijbiomac.2025.146679.

Data availability

Data will be made available on request.

References

[1] Q. Meng, Y. Li, Q. Wang, Y. Wang, K. Li, S. Chen, P. Ling, S. Wu, Recent advances of electrospun nanofiber-enhanced hydrogel composite scaffolds in tissue engineering, J. Manuf. Process. 123 (2024) 112–127, https://doi.org/10.1016/j.jmapro.2024.05.085.

[2] Y. Li, P. Ren, Z. Sun, R. Xue, D. Ding, W. Tian, F. Ren, Y. Jin, Z. Chen, G. Zhu, High-strength, anti-fatigue, cellulose nanofiber reinforced polyvinyl alcohol based ionic conductive hydrogels for flexible strain/pressure sensors and triboelectric nanogenerators, J. Colloid Interface Sci. 669 (2024) 248–257, https://doi.org/10.1016/j.jcis.2024.05.011.

[3] Z. Zhang, W. Wang, Y. Li, K. Fu, X. Tong, B. Cao, B. Chen, 3D printing of cellulose nanofiber/polylactic acid composites via an efficient dispersion method, Compos. Commun. 43 (2023) 101731, https://doi.org/10.1016/j.coco.2023.101731.

[4] L. Li, B. Wang, M.H. Hubler, Carbon nanofibers (CNFs) dispersed in ultra-high performance concrete (UHPC): mechanical property, workability and permeability investigation, Cem. Concr. Compos. 131 (2022) 104592, https://doi.org/10.1016/j.cemconcomp.2022.104592.

[5] Z. Xie, M. Gao, A.O. Lobo, T.J. Webster, 3D bioprinting in tissue engineering for medical applications: the classic and the hybrid, Polymers 12 (2020) 1717, https://doi.org/10.3390/polym12081717.

[6] S. Liu, L. Cheng, Y. Liu, H. Zhang, Y. Song, J.-H. Park, K. Dashnyam, J.-H. Lee, F.A.-H. Khalak, O. Riester, Z. Shi, S. Ostrovidov, H. Kaji, H.-P. Deigner, J.L. Pedraz, J. C. Knowles, Q. Hu, H.-W. Kim, M. Ramalingam, 3D bioprinting tissue analogs: current development and translational implications, J. Tissue Eng. 14 (2023), https://doi.org/10.1177/20417314231187113, 20417314231187113.

[7] G. Decante, J.B. Costa, J. Silva-Correia, M.N. Collins, R.L. Reis, J.M. Oliveira, Engineering bioinks for 3D bioprinting, Biofabrication 13 (2021) 032001, https://doi.org/10.1088/1758-5090/abec2c.

[8] S. Sakai, S. Yamamoto, R. Hirami, M. Hidaka, K. Chamara Manoj Lakmal Elvitigala, Enzymatically gellable chitosan inks with enhanced printability by chitosan nanofibers for 3D printing of wound dressings, Eur. Polym. J. 210 (2024) 112960, https://doi.org/10.1016/j.eurpolymj.2024.112960.
[9] S. Sakai, A. Yoshii, S. Sakurai, K. Horii, O. Nagasuna, Silk fibroin nanofibers: a promising ink additive for extrusion three-dimensional bioprinting, Mater. Today Bio 8 (2020) 100078, https://doi.org/10.1016/j.mtbio.2020.100078.
[10] A. Sharma, T. Mandal, S. Goswami, Dispersibility and stability studies of cellulose nanofibers: implications for nanocomposite preparation, J. Polym. Environ. 29 (2021) 1516–1525, https://doi.org/10.1007/s10924-020-01974-7.
[11] J. Kim, J. Bang, Y. Kim, J.-C. Kim, S.-W. Hwang, H. Yeo, I.-G. Choi, H.W. Kwak, Eco-friendly alkaline lignin/cellulose nanofiber drying system for efficient redispersion behavior, Carbohydr. Polym. 282 (2022) 119122, https://doi.org/10.1016/j.carbpol.2022.119122.
[12] L. Xiaorui, Z. Fuyin, W. Xudong, G. Xuezheng, Z. Shudong, L. Hui, D. Dandan, L. Yubing, W. Lizhen, F. Yubo, Biomaterial inks for extrusion-based 3D bioprinting: property, classification, modification, and selection, Int. J. Bioprinting 9 (2022) 649, https://doi.org/10.18063/ijb.v9i2.649.
[13] X. Cui, J. Li, Y. Hartanto, M. Durham, J. Tang, H. Zhang, G. Hooper, K. Lim, T. Woodfield, Advances in extrusion 3D bioprinting: a focus on multicomponent hydrogel-based bioinks, Adv. Healthc. Mater. 9 (2020) 1901648, https://doi.org/10.1002/adhm.201901648.
[14] S.R. Pardeshi, N.S. Deshmukh, D.R. Telange, S.N. Nangare, Y.Y. Sonar, S. H. Lakade, M.T. Harde, C.V. Pardeshi, A. Gholap, P.K. Deshmukh, M.P. More, Process development and quality attributes for the freeze-drying process in pharmaceuticals, biopharmaceuticals and nanomedicine delivery: a state-of-the-art review, Future J. Pharm. Sci. 9 (2023) 99, https://doi.org/10.1186/s43094-023-00551-8.
[15] I. Déléris, J. Wallecan, Relationship between processing history and functionality recovery after rehydration of dried cellulose-based suspensions: a critical review, Adv. Colloid Interface Sci. 246 (2017) 1–12, https://doi.org/10.1016/j.cis.2017.06.013.
[16] P. Posada, J. Velásquez-Cock, C. Gómez-Hoyos, A.M. Serpa Guerra, S.V. Lyulin, J. M. Kenny, P. Gañán, C. Castro, R. Zuluaga, Drying and redispersion of plant cellulose nanofibers for industrial applications: a review, Cellulose 27 (2020) 10649–10670, https://doi.org/10.1007/s10570-020-03348-7.
[17] S. Shin, S. Park, M. Park, E. Jeong, K. Na, H.J. Youn, J. Hyun, Cellulose nanofibers for the enhancement of printability of low viscosity gelatin derivatives, BioResources 12 (2017) 2941–2954.
[18] R. Priyadarshi, J.-W. Rhim, Chitosan-based biodegradable functional films for food packaging applications, Innov. Food Sci. Emerg. Technol. 62 (2020) 102346, https://doi.org/10.1016/j.ifset.2020.102346.
[19] S. Bonde, C. Chandarana, P. Prajapati, V. Vashi, A comprehensive review on recent progress in chitosan composite gels for biomedical uses, Int. J. Biol. Macromol. 272 (2024) 132723, https://doi.org/10.1016/j.ijbiomac.2024.132723.
[20] M. Peifen, L. Mengyun, H. Jinglong, L. Danqian, T. Yan, X. Liwei, Z. Han, D. Jianlong, L. Lingyan, Z. Guanghui, W. Zhiping, New skin tissue engineering scaffold with sulfated silk fibroin/chitosan/hydroxyapatite and its application, Biochem. Biophys. Res. Commun. 640 (2023) 117–124, https://doi.org/10.1016/j.bbrc.2022.11.086.
[21] M.F. de Souza, H.N. da Silva, J.F.B. de Rodrigues, M.D.M. Macêdo, W.J.B. de Sousa, R.C. Barbosa, M.V.L. Fook, Chitosan/gelatin scaffolds loaded with *Jatropha mollissima* extract as potential skin tissue engineering materials, Polymers 15 (2023) 603, https://doi.org/10.3390/polym15030603.
[22] M. Saeedi, K. Morteza-Semnani, A. Siahposht-Khachaki, J. Akbari, M. Valizadeh, A. Sanaee, B. Jafarkhani, M. Eghbali, H.H.H. Zanjani, S.M.H. Hashemi, S. M. Rahimnia, Passive targeted drug delivery of venlafaxine HCl to the brain by modified chitosan nanoparticles: characterization, cellular safety assessment, and in vivo evaluation, J. Pharm. Innov. 18 (2023) 1441–1453, https://doi.org/10.1007/s12247-023-09733-6.
[23] M. Gaur, S. Maurya, Mohd.S. Akhtar, A.B. Yadav, Synthesis and evaluation of BSA-loaded PLGA–chitosan composite nanoparticles for the protein-based drug delivery system, ACS Omega 8 (2023) 18751–18759, https://doi.org/10.1021/acsomega.3c00738.
[24] Y. Liu, J. Chen, P. Li, N. Ning, The effect of chitosan in wound healing: a systematic review, Adv. Skin Wound Care 34 (2021) 262, https://doi.org/10.1097/01.ASW.0000723128.58588.b5.
[25] J. Zhao, P. Qiu, Y. Wang, Y. Wang, J. Zhou, B. Zhang, L. Zhang, D. Gou, Chitosan-based hydrogel wound dressing: from mechanism to applications, a review, Int. J. Biol. Macromol. 244 (2023) 125250, https://doi.org/10.1016/j.ijbiomac.2023.125250.
[26] C. Ni, Z. Zhang, Y. Wang, Z. Zhang, X. Guo, H. Lv, Hyaluronic acid and HA-modified cationic liposomes for promoting skin penetration and retention, J. Control. Release 357 (2023) 432–443, https://doi.org/10.1016/j.jconrel.2023.03.049.
[27] S.S. Hakki, S.B. Bozkurt, A. Sculean, D. Božić, Hyaluronic acid enhances cell migration, viability, and mineralized tissue-specific genes in cementoblasts, J. Periodontal Res. 59 (2024) 63–73, https://doi.org/10.1111/jre.13201.
[28] W. Mubarok, C. Zhang, S. Sakai, 3D bioprinting of sugar beet pectin through horseradish peroxidase-catalyzed cross-linking, ACS Appl. Bio Mater. 7 (2024) 3506–3514, https://doi.org/10.1021/acsabm.4c00418.
[29] S. Sakai, K. Ueda, E. Gantumur, M. Taya, M. Nakamura, Drop-on-drop multimaterial 3D bioprinting realized by peroxidase-mediated cross-linking, Macromol. Rapid Commun. 39 (2018) 1700534, https://doi.org/10.1002/marc.201700534.
[30] A. Shavandi, S. Hosseini, O.V. Okoro, L. Nie, F. Eghbali Babadi, F. Melchels, 3D bioprinting of lignocellulosic biomaterials, Adv. Healthc. Mater. 9 (2020) 2001472, https://doi.org/10.1002/adhm.202001472.
[31] M. Pitton, A. Fiorati, S. Buscemi, L. Melone, S. Farè, N. Contessi Negrini, 3D bioprinting of pectin-cellulose nanofibers multicomponent bioinks, Front. Bioeng. Biotechnol. 9 (2021), https://doi.org/10.3389/fbioe.2021.732689.
[32] K. Ogura, C. Brasselet, G. Cabrera-Barjas, M. Hamidi, A. Shavandi, M. Dols-Lafargue, N. Sawamura, C. Delattre, Production of fungal nanochitosan using high-pressure water jet system for biomedical applications, Materials 15 (2022) 1375, https://doi.org/10.3390/ma15041375.
[33] M. Khanmohammadi, S. Sakai, M. Taya, Impact of immobilizing of low molecular weight hyaluronic acid within gelatin-based hydrogel through enzymatic reaction on behavior of enclosed endothelial cells, Int. J. Biol. Macromol. 97 (2017) 308–316, https://doi.org/10.1016/j.ijbiomac.2016.12.088.
[34] M. Hidaka, S. Sakai, Photo- and Schiff base-crosslinkable chitosan/oxidized glucomannan composite hydrogel for 3D bioprinting, Polysaccharides 6 (2025) 19, https://doi.org/10.3390/polysaccharides6010019.
[35] W. Mubarok, K.C.M.L. Elvitigala, S. Sakai, Tuning myogenesis by controlling gelatin hydrogel properties through hydrogen peroxide-mediated cross-linking and degradation, Gels 8 (2022) 387, https://doi.org/10.3390/gels8060387.
[36] S. Sakai, M. Khanmohammadi, A.B. Khoshfetrat, M. Taya, Horseradish peroxidase-catalyzed formation of hydrogels from chitosan and poly(vinyl alcohol) derivatives both possessing phenolic hydroxyl groups, Carbohydr. Polym. 111 (2014) 404–409, https://doi.org/10.1016/j.carbpol.2014.05.010.
[37] S. Sakai, K. Mochizuki, Y. Qu, M. Mail, M. Nakahata, M. Taya, Peroxidase-catalyzed microextrusion bioprinting of cell-laden hydrogel constructs in vaporized ppm-level hydrogen peroxide, Biofabrication 10 (2018) 045007, https://doi.org/10.1088/1758-5090/aadc9e.
[38] S. Sakai, T. Kotani, R. Harada, R. Goto, T. Morita, S. Bouissil, P. Dubessay, G. Pierre, P. Michaud, R. El Boutachfaiti, M. Nakahata, M. Kojima, E. Petit, C. Delattre, Development of phenol-grafted polyglucuronic acid and its application to extrusion-based bioprinting inks, Carbohydr. Polym. 277 (2022) 118820, https://doi.org/10.1016/j.carbpol.2021.118820.
[39] Z. Fu, S. Naghieh, C. Xu, C. Wang, W. Sun, X. Chen, Printability in extrusion bioprinting, Biofabrication 13 (2021) 033001, https://doi.org/10.1088/1758-5090/abe7ab.
[40] S.A. Wilson, L.M. Cross, C.W. Peak, A.K. Gaharwar, Shear-thinning and thermo-reversible nanoengineered inks for 3D bioprinting, ACS Appl. Mater. Interfaces 9 (2017) 43449–43458, https://doi.org/10.1021/acsami.7b13602.
[41] Y. Chen, X. Xiong, X. Liu, R. Cui, C. Wang, G. Zhao, W. Zhi, M. Lu, K. Duan, J. Weng, S. Qu, J. Ge, 3D bioprinting of shear-thinning hybrid bioinks with excellent bioactivity derived from gellan/alginate and thixotropic magnesium phosphate-based gels, J. Mater. Chem. B 8 (2020) 5500–5514, https://doi.org/10.1039/D0TB00060D.
[42] R.H. Rakin, H. Kumar, A. Rajeev, G. Natale, F. Menard, I.T.S. Li, K. Kim, Tunable metacrylated hyaluronic acid-based hybrid bioinks for stereolithography 3D bioprinting, Biofabrication 13 (2021) 044109, https://doi.org/10.1088/1758-5090/ac25cb.
[43] K. Missoum, J. Bras, M.N. Belgacem, Water redispersible dried nanofibrillated cellulose by adding sodium chloride, Biomacromolecules 13 (2012) 4118–4125, https://doi.org/10.1021/bm301378n.
[44] L. Ouyang, R. Yao, Y. Zhao, W. Sun, Effect of bioink properties on printability and cell viability for 3D bioplotting of embryonic stem cells, Biofabrication 8 (2016) 035020, https://doi.org/10.1088/1758-5090/8/3/035020.
[45] Y. Luo, X. Wei, P. Huang, 3D bioprinting of hydrogel-based biomimetic microenvironments, J. Biomed. Mater. Res. B Appl. Biomater. 107 (2019) 1695–1705, https://doi.org/10.1002/jbm.b.34262.
[46] M.B. Łabowska, K. Cierluk, A.M. Jankowska, J. Kulbacka, J. Detyna, I. Michalak, A review on the adaption of alginate-gelatin hydrogels for 3D cultures and bioprinting, Materials 14 (2021) 858, https://doi.org/10.3390/ma14040858.
[47] S. Sakai, H. Ohi, M. Taya, Gelatin/hyaluronic acid content in hydrogels obtained through blue light-induced gelation affects hydrogel properties and adipose stem cell behaviors, Biomolecules 9 (2019) 342, https://doi.org/10.3390/biom9080342.
[48] A. Sugawara-Narutaki, S. Yasunaga, Y. Sugioka, D.H.T. Le, I. Kitamura, J. Nakamura, C. Ohtsuki, Rheology of dispersions of high-aspect-ratio nanofibers assembled from elastin-like double-hydrophobic polypeptides, Int. J. Mol. Sci. 20 (2019) 6262, https://doi.org/10.3390/ijms20246262.
[49] X. Li, B. Zhao, Y. Zou, G. Guo, J. Li, J. Sheng, Y. Tian, J. Luo, Structure, rheology and stability of walnut oleogels structured by cellulose nanofiber of different lengths, Food Hydrocoll. 154 (2024) 110148, https://doi.org/10.1016/j.foodhyd.2024.110148.